Supporting Information

Topological Chemical Transition Strategy of Bismuth-based Materials for High-efficient Electrocatalytic Carbon Dioxide Conversion to Formate

Runze Ye, Yun Tong, Dongmei Feng and Pengzuo Chen**

Department of Chemistry, Key Laboratory of Surface & Interface Science of Polymer Materials of Zhejiang Province, Zhejiang Sci-Tech University, 928 Second Avenue, Xiasha High Education Zone, Hangzhou 310018, (P. R. China)

Correspondence and requests for materials should be addressed to Y. Tong (E-mail: tongyun@mail.ustc.edu.cn; pzchen@zstu.edu.cn)

Table of contents

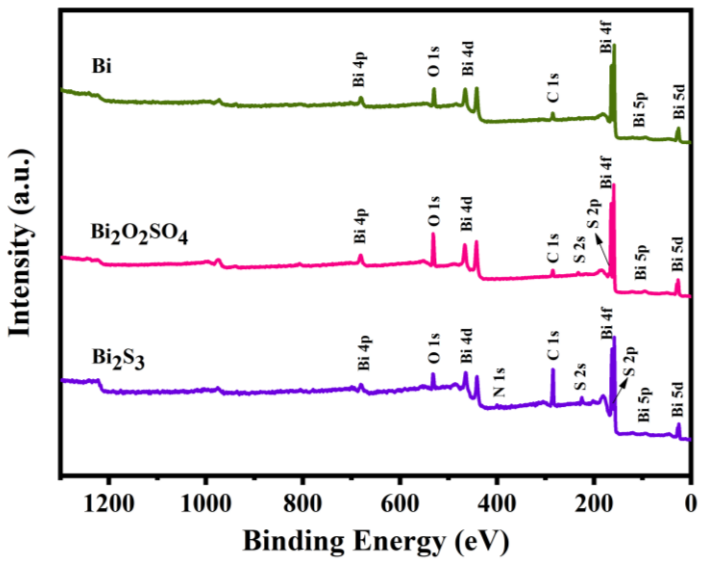

Figure S1. XPS survey spectrum of Bi_2S_3, $Bi_2O_2SO_4$, and metal Bi samples.

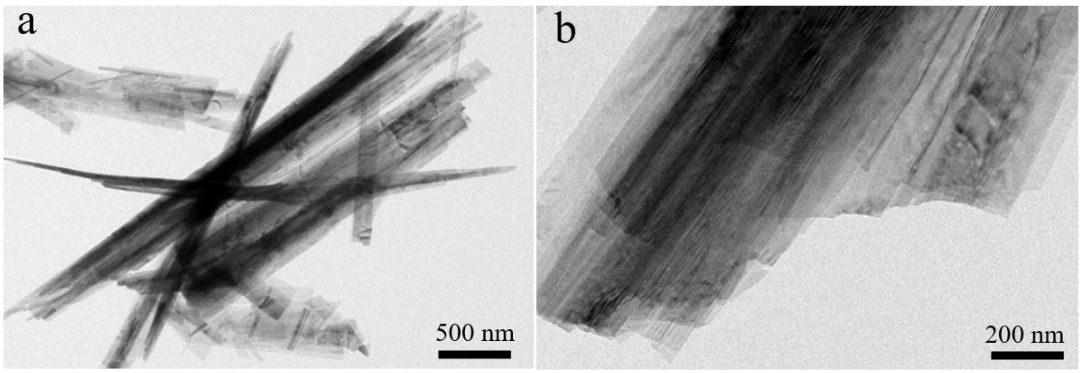

Figure S2. (a-b) The TEM images of Bi_2S_3 precursor.

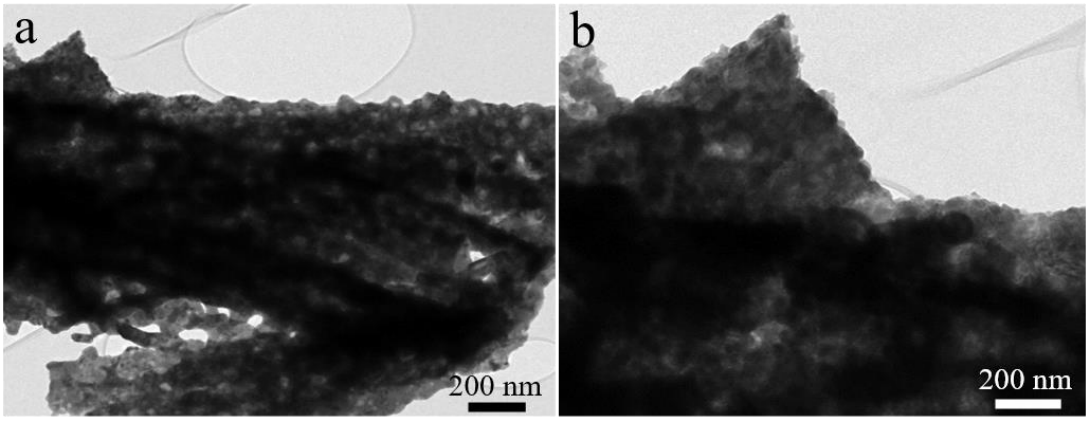

Figure S3. (a-b) The TEM images of $Bi_2O_2SO_4$.

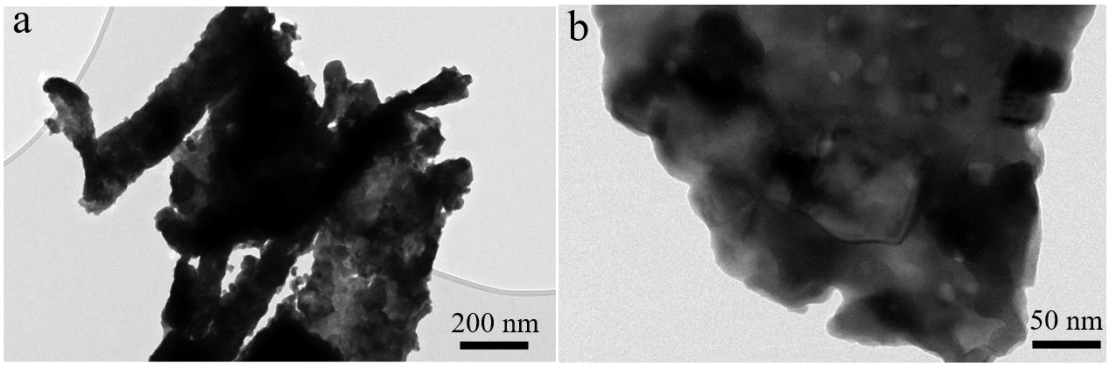

Figure S4. (a-b) The TEM images of metal Bi.

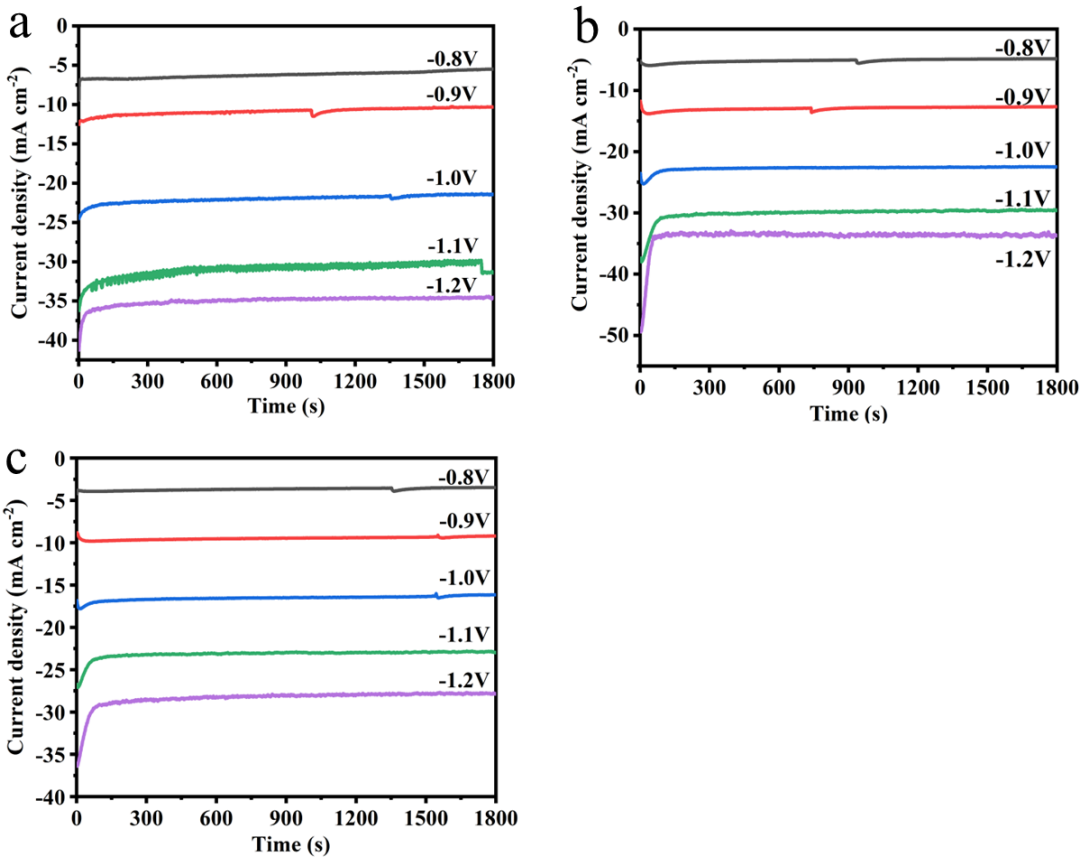

Figure S5. Constant potential electrolysis of (a) Bi_2S_3, (b) $Bi_2O_2SO_4$ and (c) Bi at each applied potential in CO_2 saturated 0.5 M $KHCO_3$.

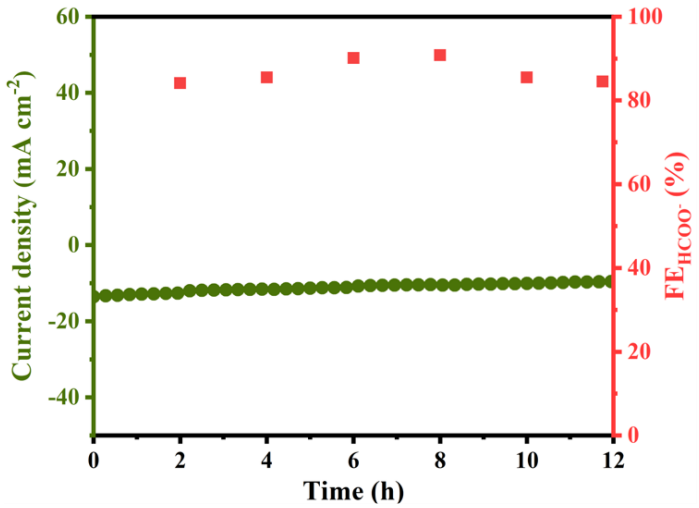

Figure S6. Stability test of the Bi catalyst at -0.9 V vs. RHE.

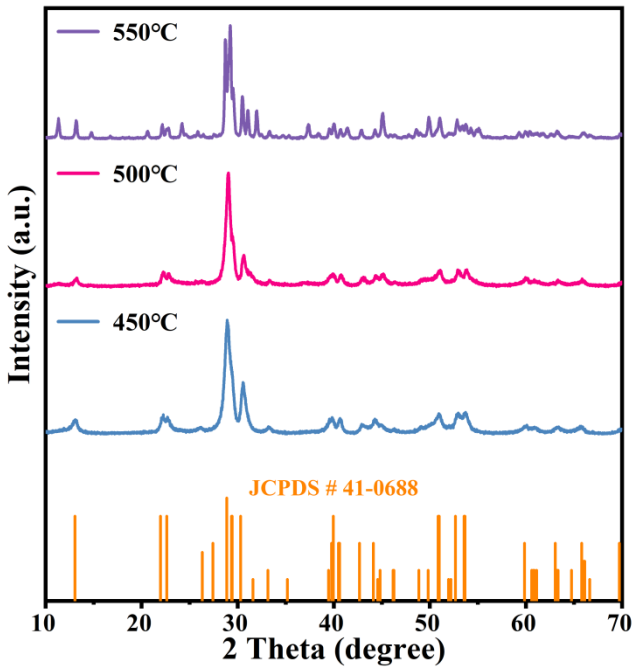

Figure S7. The XRD patterns of the $Bi_2O_2SO_4$ samples were synthesized at different reaction temperatures.

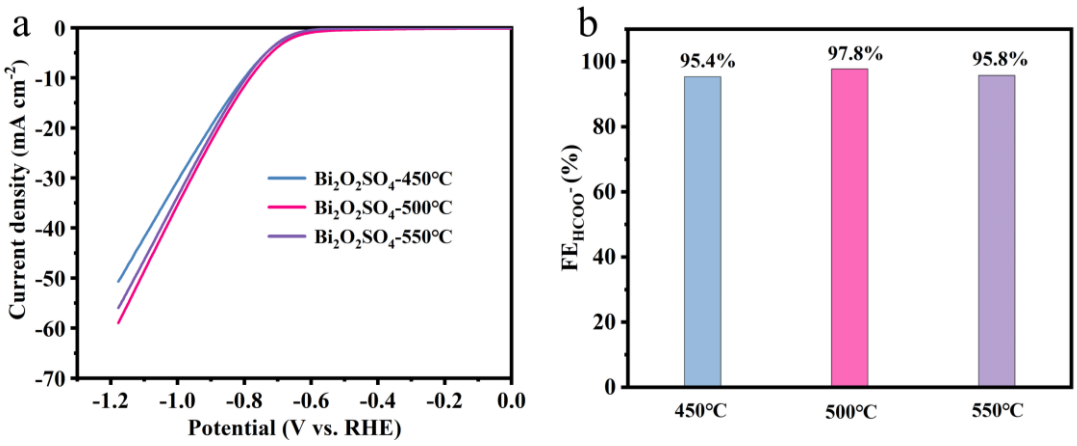

Figure S8. (a) LSV curves of the $Bi_2O_2SO_4$ samples that were synthesized at different reaction temperatures. (b) Corresponding FEs of these samples at -0.8 V.

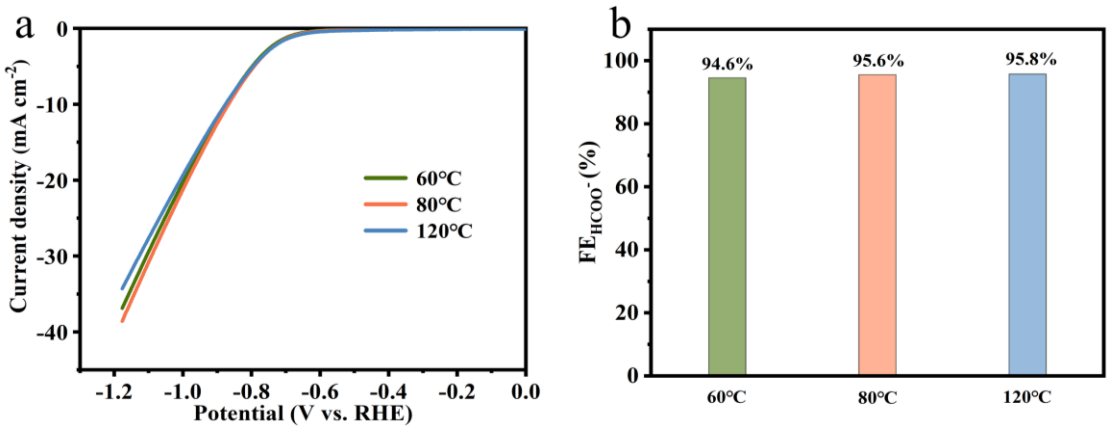

Figure S9. (a) LSV curves of the surface treated Bi sample at different temperatures in air. (b) Corresponding FEs of these samples at -1.0 V.

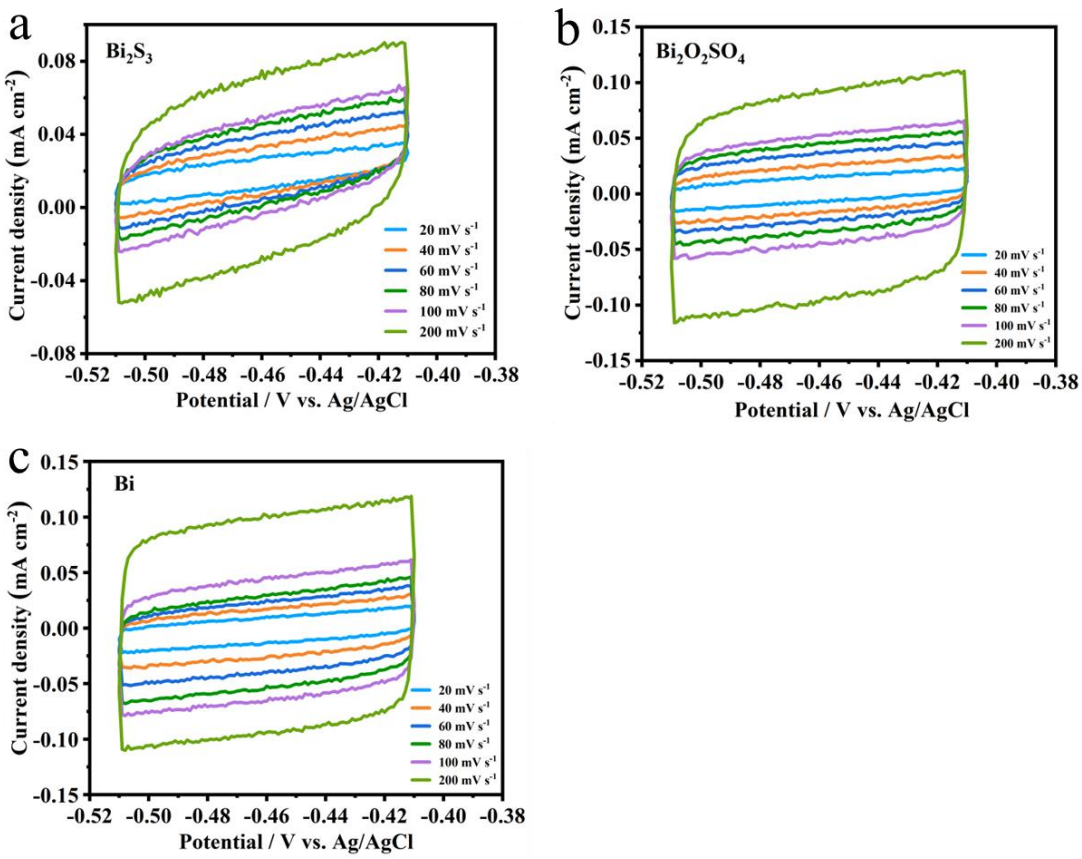

Figure S10. The CV curves of (a) Bi_2S_3, (b) $Bi_2O_2SO_4$, and (c) Bi samples in 0.5 M $KHCO_3$ at scan rates of 20, 40, 60, 80,100, 200 mV s^{-1}, respectively.

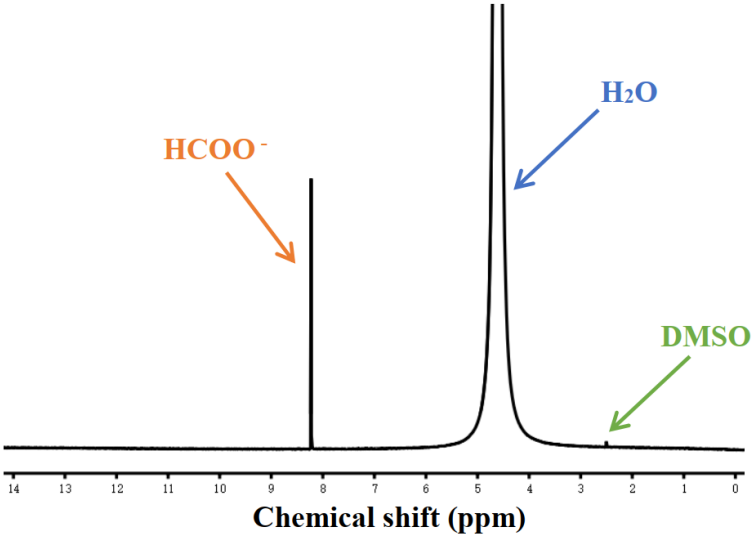

Figure S11. ^{1}H NMR spectra of $Bi_2O_2SO_4$ catalyst after the electrocatalytic CO_2 reduction in a flow cell.

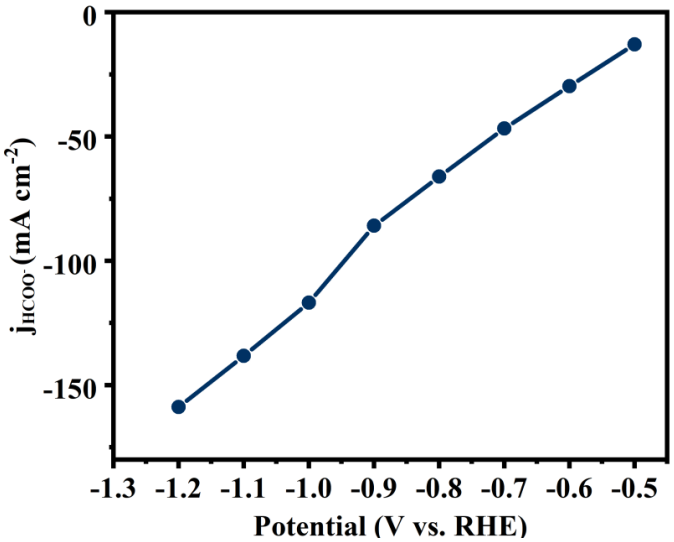

Figure S12. The partial current density of formate for $Bi_2O_2SO_4$ catalyst at different applied potentials in a flow cell.

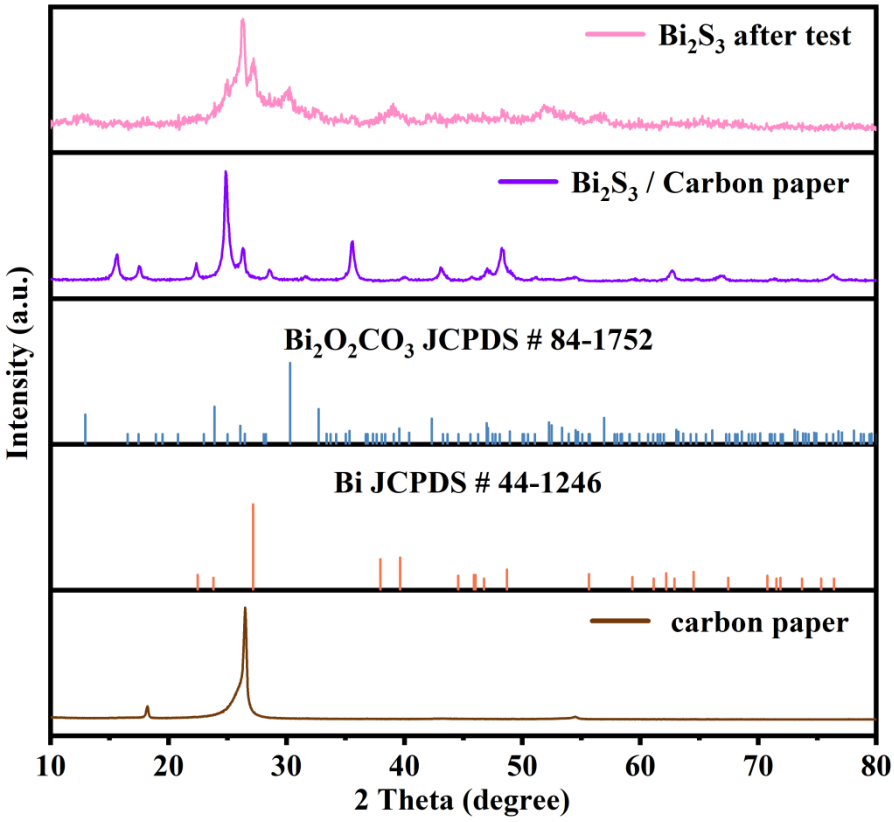

Figure S13. The XRD pattern of Bi_2S_3 catalyst on carbon paper before and after the electrocatalytic CO_2 reduction.

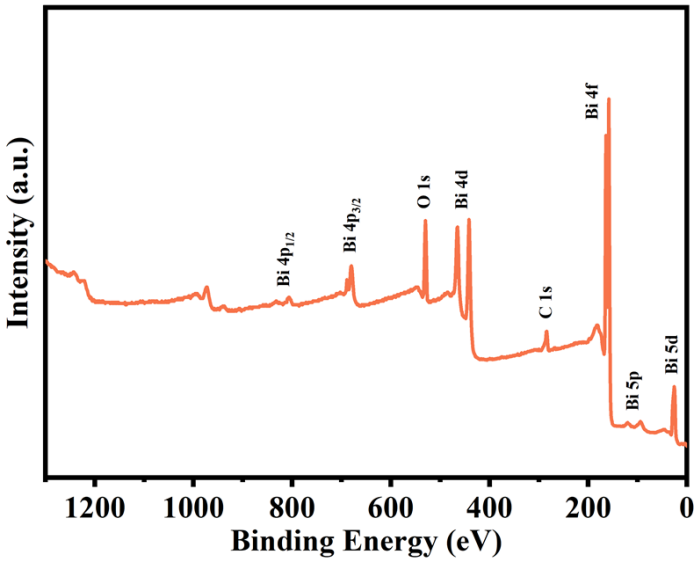

Figure S14. The XPS survey of $Bi_2O_2SO_4$ catalyst after the electrocatalytic CO_2 reduction.

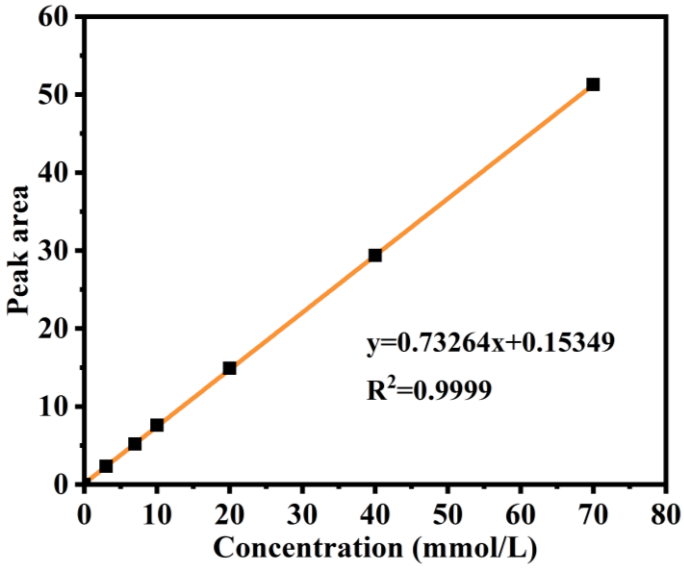

Figure S15. The NMR calibration curve of DMSO.

Table S1. Relevant parameters of Bi and $Bi_2O_2SO_4$ samples at -0.9 V vs. RHE.

Sample	$j_{formate}$ at -0.9 V vs. RHE (mA cm^{-2})	C_{dl} (mF cm^{-2})	$j_{formate}'$ at -0.9 V vs. RHE per C_{dl} (mA cm^{-2})
Bi	**8.53**	**0.48**	**17.77**
$Bi_2O_2SO_4$	**12.56**	**0.46**	**27.3**

Table S2. Comparison of $Bi_2O_2SO_4$ with recently reported Bi-based electrocatalysts in H-type cell.

Catalyst	Electrolyte	Maximum $FE_{formate}$ with the applied potential (vs. RHE)	Potential ranges (mV) for $FE_{formate}$ > 80%	Ref
$Bi_2O_2SO_4$ reduced Bi	**0.5 M $KHCO_3$**	**97% at -0.9 V**	**400**	**This work**
OD-BiNSs	**0.5 M $KHCO_3$**	**93% at -0.95 V**	**200**	**[1]**
Pits-Bi NS	**0.1 M $KHCO_3$**	**95.3% at -1.14V**	**400**	**[2]**
2D Bi NSs	**0.5 M $KHCO_3$**	**95% at -0.9 V**	**400**	**[3]**
Bi nanosheets	**0.5 M $KHCO_3$**	**91.3% at -1.0 V**	**600**	**[4]**
Bi–BTB	**0.5 M $KHCO_3$**	**96.1% at -0.669 V**	**500**	**[5]**
Bi Nanotubes	**0.5 M $KHCO_3$**	**97% at -1.0 V**	**600**	**[6]**
Mesoporous Bi NSs	**0.5 M $KHCO_3$**	**95.9% at -0.77 V**	**300**	**[7]**
Bi nanostructure	**0.5 M $KHCO_3$**	**92% at -0.9 V**	**400**	**[8]**
SD-Bi	**0.5 M $NaHCO_3$**	**84.0% at -0.75 V**	**200**	**[9]**
2D Bi NSs	**0.1 M $KHCO_3$**	**86.0% at -1.1 V**	**200**	**[10]**

Table S3. Comparison of $Bi_2O_2SO_4$ with recently reported electrocatalysts in a flow cell.

Catalyst	Electrolyte	Maximum $FE_{formate}$ with the applied potential (vs. RHE)	Potential ranges (mV) for $FE_{formate}$ > 90%	Ref
$Bi_2O_2SO_4$ reduced Bi	1.0 M KOH	97.2% at -1.2V	700	This work
InS Nanorods	1.0 M KOH	94% at - 0.7 V	500	[11]
Bi_2O_3@C-800	1.0 M KOH	95% at -0.7 V	700	[12]
Bi-300	1.0 M KOH	100% at -0.7 V	100	[13]
InN nanosheet	1.0 M KOH	91% at -0.9V	100	[14]
Bi-SnO_x	1.0 M KOH	94.6 % at -0.51 V	200	[15]
SnO_2-Bi_2O_3	1.0 M KOH	91% at -1.29 V	100	[16]
Bi@Sn NPs	2.0 M $KHCO_3$	95% at -1.02 V	350	[17]
Bi NRs	1.0 M KOH	>95%	600	[18]
In-Sn alloy	1.0 M KOH	94% at -0.98 V	550	[19]
$ZnIn_2S_4$	1.0 M $KHCO_3$	99.3% at -1.18 V	300	[20]

References:

[1] Lee J, Liu H, Chen Y, et al. Bismuth Nanosheets Derived by In Situ Morphology Transformation of Bismuth Oxides for Selective Electrochemical CO_2 Reduction to Formate. *ACS Appl. Mater. Interfaces*, **2022**, *14(12): 14210-14217*.

[2] Yuan Y, Wang Q, Qiao Y, et al. In Situ Structural Reconstruction to Generate the Active Sites for CO_2 Electroreduction on Bismuth Ultrathin Nanosheets. *Adv. Mater*, **2022**, *12(29): 2200970.*

[3] Liu P, Liu H, Zhang S, et al. A general strategy for obtaining BiO_X nanoplates derived Bi nanosheets as efficient CO_2 reduction catalysts by enhancing $CO_2^{\bullet-}$ adsorption and electron transfer. *J. Colloid Interface Sci.*, **2021**, *602: 740-747*.

[4] Wang D, Wang Y, Chang K, et al. Residual iodine on in-situ transformed bismuth nanosheets induced activity difference in CO_2 electroreduction. *J. CO_2 Util.*, **2022**, *55: 101802.*

[5] Yuan W W, Wu J X, Zhang X D, et al. In situ transformation of bismuth metal–organic frameworks for efficient selective electroreduction of CO_2 to formate. *J. Mater. Chem. A*, **2020**, *8(46): 24486-24492*.

[6] Fan K, Jia Y, Ji Y, et al. Curved surface boosts electrochemical CO_2 reduction to formate via bismuth nanotubes in a wide potential window. *ACS Catal*, **2019**, *10(1): 358-364*.

[7] Wu D, Liu J, Liang Y, et al. Electrochemical Transformation of Facet-Controlled BiOI into Mesoporous Bismuth Nanosheets for Selective Electrocatalytic Reduction of CO_2 to Formic Acid. *ChemSusChem*, **2019**, *12(20): 4700-4707*.

[8] Lu P, Gao D, He H, et al. Facile synthesis of a bismuth nanostructure with enhanced selectivity for electrochemical conversion of CO_2 to formate. *Nanoscale*, **2019**, *11(16): 7805-7812*.

[9] Zhang Y, Li F, Zhang X, et al. Electrochemical reduction of CO_2 on defect-rich Bi derived from Bi_2S_3 with enhanced formate selectivity. *J. Mater. Chem. A*, **2018**, *6(11): 4714-4720.*

[10] Zhang W, Hu Y, Ma L, et al. Liquid-phase exfoliated ultrathin Bi nanosheets:

uncovering the origins of enhanced electrocatalytic CO_2 reduction on two-dimensional metal nanostructure. *Nano Energy,* **2018**, *53: 808-816*.

[11] Zhang Y, Lan J, Xie F, et al. Aligned InS Nanorods for Efficient Electrocatalytic Carbon Dioxide Reduction. *ACS Appl. Mater. Interfaces*, **2022**, *14(22), 25257-25266*.

[12] Yi L, Chen J, Shao P, et al. Molten-salt-assisted synthesis of bismuth nanosheets for long-term continuous electrocatalytic conversion of CO_2 to formate. *Angew. Chem. Int. Ed.*, **2020**, *59(45): 20112-20119*.

[13] Deng P, Yang F, Wang Z, et al. Metal–Organic Framework-Derived Carbon Nanorods Encapsulating Bismuth Oxides for Rapid and Selective CO_2 Electroreduction to Formate. *Angew. Chem. Int. Ed.*, **2020**, *132(27): 10899 - 10905*.

[14] Zhang A, Liang Y, Li H, et al. In-situ surface reconstruction of InN nanosheets for efficient CO_2 electroreduction into formate. *Nano Lett.*, **2020**, *20(11): 8229-8235*.

[15] Yang Q, Wu Q, Liu Y, et al. Novel Bi-Doped Amorphous SnO_x Nanoshells for Efficient Electrochemical CO_2 Reduction into Formate at Low Overpotentials. *Adv. Mater*, **2020**, *32(36): 2002822*.

[16] Wang X, Wang W, Zhang J, et al. Carbon sustained SnO_2-Bi_2O_3 hollow nanofibers as Janus catalyst for high-efficiency CO_2 electroreduction. *Chem. Eng. J.*, **2021**, *426: 131867*.

[17] Xing Y, Kong X, Guo X, et al. Bi@Sn core–shell structure with compressive strain boosts the electroreduction of CO_2 into formic acid. *Adv. Sci.*, **2020**, *7(22): 1902989*.

[18] Li Y, Chen J, Chen S, et al. In Situ Confined Growth of Bismuth Nanoribbons with Active and Robust Edge Sites for Boosted CO_2 Electroreduction. *ACS Energy Lett.*, **2022**, *7(4): 1454-1461*.

[19] Wang J, Ning S, Luo M, et al. In-Sn alloy core-shell nanoparticles: In-doped SnO_x shell enables high stability and activity towards selective formate production from electrochemical reduction of CO_2. *Appl. Catal. B*, **2021**, *288:119979*.

[20] Chi L P, Niu Z Z, Zhang X L, et al. Stabilizing indium sulfide for CO_2 electroreduction to formate at high rate by zinc incorporation. *Nat. Commun*, **2021**, *12(1): 1-9*.